CrystEngComm

Cite this: *CrystEngComm*, 2012, **14**, 1031

www.rsc.org/crystengcomm

PAPER

Synthesis and characterization of thienyl-substituted pyridinium salts for second-order nonlinear optics†

Liang Li,[a] Huijuan Cui,[a] Zhou Yang,*[a] Xutang Tao,[b] Xinsong Lin,[c] Ning Ye[c] and Huai Yang*[a]

Received 9th September 2011, Accepted 19th October 2011
DOI: 10.1039/c1ce06177a

The synthesis of a series of thienyl-substituted pyridinium salts with different counter-anions and their second-order nonlinear optical (NLO) properties are described. Kurtz powder tests revealed that, out of the twelve new pyridinium salts, four possess noncentrosymmetric structures and the maximum powder second harmonic generation (SHG) efficiency is 0.6 times of DAST. Single crystals of three new salts were successfully obtained from methanol by slow evaporation method. X-Ray studies exhibited that they crystallized in the monoclinic space group $P2_1/c$, $P2_1$, and $P2_1/n$, respectively. (*E*)-4-(2-(5-(dimethylamino)thiophen-2-yl)vinyl)-1-methylpyridinium 4-hydroxybenzenesulfonate (**3c**) forms a hydrated noncentrosymmetric phase with a large macroscopic optical nonlinearity 0.5 times of that of DAST at the non-resonant wavelength of $\lambda = 2109$ nm, while both (*E*)-4-(2-(5-(dimethylamino) thiophen-2-yl)vinyl)-1-methylpyridinium 2-amino-3,5-dimethylbenzenesulfonate (**3i**) and (*E*)-4-(2-(5-(dimethylamino)thiophen-2-yl)vinyl)-1-methylpyridinium iodide (**3a**) crystallize in centrosymmetric structures.

Introduction

Much effort continues to be devoted to the design of new materials with large second-order optical nonlinearities, owing to their potential in various photonic applications such as frequency conversion,[1] optical parametric oscillation,[2] high-speed information processing, storage,[3] optical switching[4] and telecommunication.[5] Compared with inorganic materials, molecular organic materials have been of extensive interest due to their large nonlinear optical properties, ultrafast response times and almost unlimited design possibilities.[6,7] Among the various types of organic materials investigated worldwide, ionic organic crystals are of special interest due to their superior long-term thermal and photochemical stability combined with a high chromophore concentration. Attractive aspects of such molecular salt compounds include the possibility of exploiting counterion variations to produce noncentrosymmetric bulk crystalline structures which are a prerequisite for macroscopic second-order NLO effects.[8] For example, 4-*N*,*N*-dimethylamino-4′-*N*′-methyl-stilbazolium tosylate (DAST) with powder second harmonic generation efficiency of 1×10^3 times that of urea standard at 1907nm, exhibits a large NLO coefficient d_{11} of 330 pm V^{-1} at 1907 nm and an electro-optic coefficient r_{11} of 77 pm V^{-1} at 800 nm.[9,10] This has motivated several research groups to investigate the growth properties to achieve high-quality and large-size crystals of DAST, which is still very challenging. Moreover, the theoretical limits for the macroscopic second-order nonlinearities in organic crystals are still far from being achieved.[11] Therefore it is desirable to develop new organic materials with larger nonlinear optical properties and/or better crystal growth abilities compared with those of DAST. Molecular optimizing of stilbazolium salts has been demonstrated to be a simple and highly successful strategy to obtain materials with very high nonlinear optical properties.[12] During the course of optimization process of the molecular structure, a variety of DAST derivatives *via* amounts of anions modifying have been developed.[13–18] In our previous work, the synthesis, crystal growth and characterization of a series of stilbazolium derivatives, obtained by carefully modifying the structure with various substituent groups on the counter-anion, have been investigated.[11,15–18] Among them, DSNS[11] (4-*N*,*N*-dimethylamino-4′-*N*′-methyl-stilbazolium 2-naphthalenesulfonate) was discussed for its nonlinear optical properties, with 50% higher second-order nonlinearity compared with DAST at 1907 nm. DSTMS[16] (4-*N*,*N*-dimethylamino-4′-*N*′-methyl-stilbazolium 2,4,6-trimethylbenzenesulfonate) was developed with similar second-order susceptibilities and better growth characteristics than that of DAST. At the same time, numerous studies on changing the cation of stilbazolium compounds have been carried out, some interesting achievements have been attained.[19–25] For example, by adopting the N-aryl

[a]*Department of Materials Physics and Chemistry, School of Materials Science and Engineering, University of Science and Technology Beijing, Beijing, 100083, P. R. China. E-mail: yangz@ustb.edu.cn; Tel: +86 10 62333759*
[b]*State Key Laboratory of Crystal Material, Shandong University, Jinan, 250100, P. R. China*
[c]*Key Laboratory of Optoelectronic Materials and Physics, Fujian Institute of Research on the Structure of Matter, Chinese Academy of Sciences, Fuzhou, Fujian, 350002, P. R. China*

† CCDC reference numbers 843803–843805. For crystallographic data in CIF or other electronic format see DOI: 10.1039/c1ce06177a

stilbazolium cation, DAPSH (*trans*-4′-(dimethylamino)-*N*-phenyl-4-stilbazolium hexafluorophosphate) crystals exhibited an extremely high diagonal second-order NLO tensor element compared with that of DAST.[26]

In this work, a heterocycle, for example, the thienyl group was introduced to substitute the phenyl group of the DAS (4-*N*,*N*-dimethylamino-4′-*N*′-methyl-stilbazolium) cation, which can form a series of new pyridinium-based chromophores to extend the molecular structure of NLO materials. The effect of the heterocycle on the nonlinear properties and crystal growth abilities of the newly developed materials have been studied. So far the salts we have synthesized exhibit SHG intensities that have a maximum which is 0.6 times of DAST, and their physical properties were also investigated. The growth of bulk crystals was performed and three crystal structures of the newly developed salts were clarified.

Results and discussion

Design and synthesis of thienyl-substituted pyridinium salt derivatives

The synthetic route, chemical structures of the new thienyl-substituted pyridinium salt derivatives and their abbreviations are shown in Fig.1. To induce asymmetry of the chromophores, which is one of the strategies to promote a noncentrosymmetric structure, the thienyl group was introduced to substitute the phenyl group of the DAS cation, thus the cation chromophores of these pyridinium derivatives contain *N*-methyl pyridinium electron acceptor and dimethylaminothienyl electron donor groups connected *via* π-systems. It is expected that the newly designed molecular structure may lead to excellent nonlinear optical property.

(*E*)-4-(2-(5-(dimethylamino)thiophen-2-yl)vinyl)-1-methylpyridinium iodide(**3a**) was obtained by the condensation reaction between 4-methyl-*N*-methyl pyridinium iodide, which was prepared by 4-picoline and iodomethane, and 5-(dimethylamino) thiophene-2-carbaldehyde, synthesized by 5-bromothiophene-2-carbaldehyde and 40% dimethylamine aqueous solution in the molar ratio 1 : 3,[27,28] in the presence of piperidine as catalyst. **3b–3m** were prepared by metathesization of the iodide salt with the sodium salt of the corresponding anion, as described previously.[29,30]

Basic characterization of the thienyl-substituted pyridinium salt derivatives

The melting point, the absorption peaks λ_{max} and the SHG powder test results of the thienyl-substituted pyridinium salts obtained after the anion exchange reaction are listed in Table 1. The melting points of the chromophores were determined by differential scanning calorimetry (DSC). From melting point data, the following trend can be extracted. Compounds with naphthalenesulfonate or quinolinesulfonate, **3k** and **3l**, have higher melting points more than 250 °C compared with the benzenesulfonate derivatives. Among the benzenesulfonate derivatives, **3c** and **3j** have higher melting points than the others,

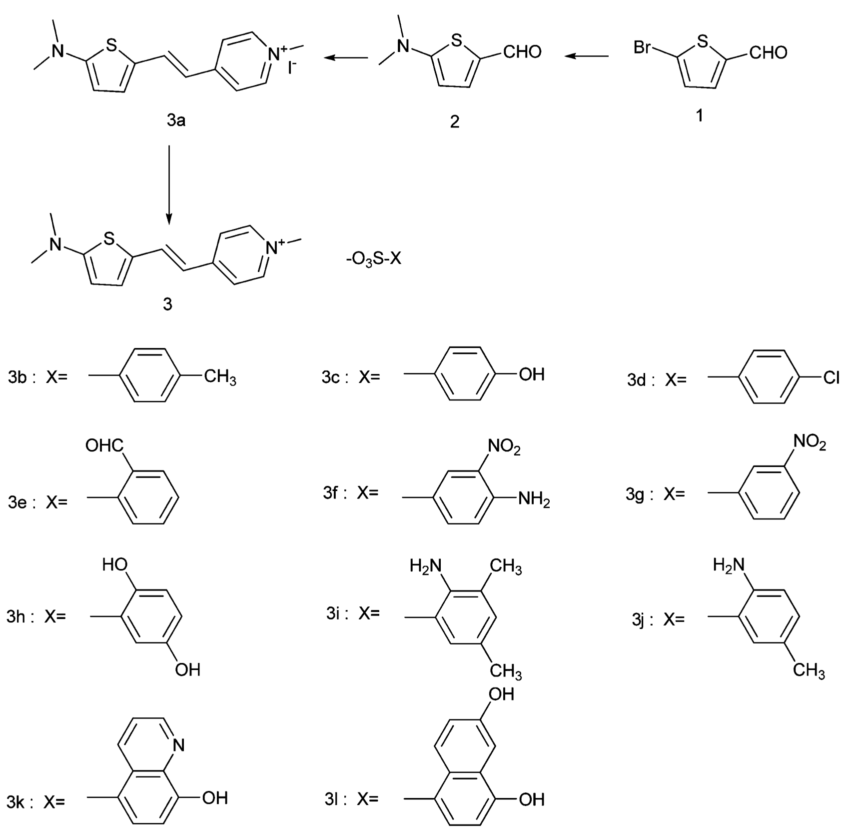

Fig. 1 The synthetic route, chemical structures and abbreviations of the new thienyl-substituted pyridinium salt derivatives.

Table 1 Physical properties of investigated compounds

Compound	Melting point (°C)	$\lambda_{max}{}^{a}$/nm	Powder SHG^{b}	Compound	Melting point (°C)	$\lambda_{max}{}^{a}$/nm	Powder SHG^{b}
3a	256 ± 1	536	0	**3g**	172 ± 1	536	0
3b	201 ± 1	536	0	**3h**	233 ± 1	536	0.02
3c	266 ± 1	536	0.50	**3i**	204 ± 1	536	0
3d	197 ± 1	536	0	**3j**	253 ± 1	536	0.60
3e	202 ± 1	536	0	**3k**	267 ± 1	536	0.08
3f	227 ± 1	536	0	**3l**	249 ± 1	536	0

^{a} In methanol at room temperature. ^{b} 2109 nm fundamental radiation, compared with DAST, with an experimental error of less than 10%.

implying that the hydroxy or amino group tendency to form hydrogen bonding seems to elevate the melting points.

The λ_{max} values in the absorption spectra of these compounds are nearly the same, which is red shifted by 60 nm compared with that of DAST (476 nm) (Fig.2). This result can be explained by the simple consideration on polarization. It was known that in the visible region, λ_{max} is determined by the cation in methanol, the change in the substituted group of the counter-anion does not affect the electronic structure of the cation chromophore. There is an increase in the electron-donating strength of the amino-substituted fragment when the thienyl group is introduced, thus resulting in red shift of λ_{max}.

The salts synthesized can be well dissolved in methanol, while they show poor solubility in other organic solvents such as dichloromethane, acetonitrile and acetone, *etc.* So methanol was selected to grow crystals as the size of the crystals depends on the amount of materials dissolved in the solvents. Take **3c** as an example, the solubility of **3c** in methanol was determined by ultraviolet spectrophotometry.[31] The relationship between the degree of absorption and concentration of the **3c** solution was measured at room temperature, which is linear and whose equation is $y = 123.01x + 0.0326$. 1 ml of saturated solution in different temperatures was diluted by 5000 times respectively to measure the degree of absorption and the corresponding solubility of **3c** was calculated. The solubility curve of **3c** in methanol is shown in Fig. 3. It can be observed that the concentration gradient of solubility was not suitable to adopt the slow cooling method, so the slow evaporation method was selected to grow **3c** crystals. Bulk **3c** crystals with a size of 7×1 mm^2 was obtained after a period of 10 days.

To investigate the macroscopic nonlinearity of the crystals, the Kurtz and Perry powder test was performed at a fundamental wavelength of 2109 nm using a tunable output of an optical parametric amplifier pumped by an amplified Nd:YAG laser. The second harmonic generation intensities of the salts compared with DAST are listed in Table 1. From this result we may expect numerous noncentrosymmetric crystal structures for the new thienyl-substituted pyridinium compounds with well-aligned chromophores, leading to large macroscopic nonlinearity and suggesting that the new series of compounds are therefore promising candidate materials for second-order nonlinear optical applications.

Single crystal structure

Of all the salts synthesized, it was found that **3c** and **3i** nucleated very easy and fast. Thin single-crystalline plates with good optical quality were able to be obtained from the recrystallization procedure. The optical quality of the crystals was investigated by placing them between a crossed polarizer (Fig.4). When the crystal was rotated around the direction of the light propagation, the linearly polarized light was transmitted when its polarization was neither parallel nor perpendicular to an axis of the optical indicatrix. These crystals appear completely opaque when at least one of the polarizers is parallel to an axis of the optical indicatrix. With this method, it can be inferred that single crystals are obtained with at least one of the main optical axes almost parallel to the plate. In order to obtain information on the crystal structures by X-ray crystallographic analysis, crystal growth of these compounds was performed in methanol by slow evaporation method at room temperature in a conical flask reflecting the solubility curves mentioned above. Bulk single crystals of **3c** and **3i** with sizes of 7×1 mm^2 and 3×2 mm^2 have been grown by this method in a period of 10 days, respectively (Fig.5).

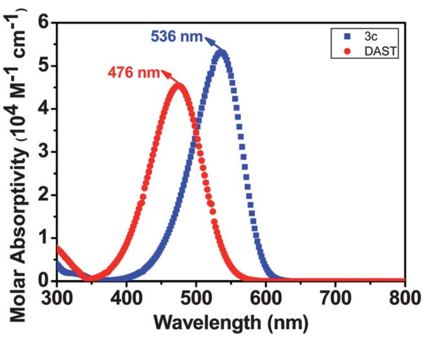

Fig. 2 Absorption spectra of **3c** and DAST in methanol.

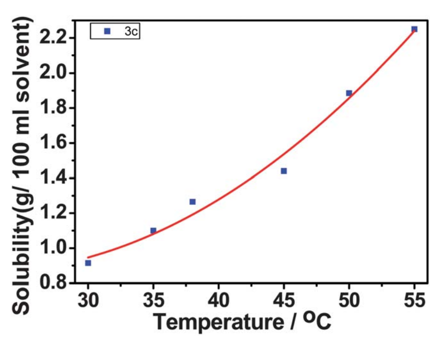

Fig. 3 Solubility/temperature curves of **3c** in methanol.

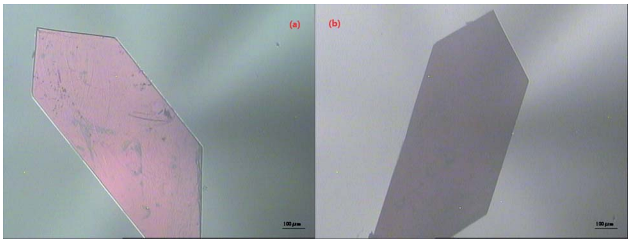

Fig. 4 **3c** crystal as observed between the crossed polarizer in a microscope. The crystal was rotated 45° from position (a) to position (b).

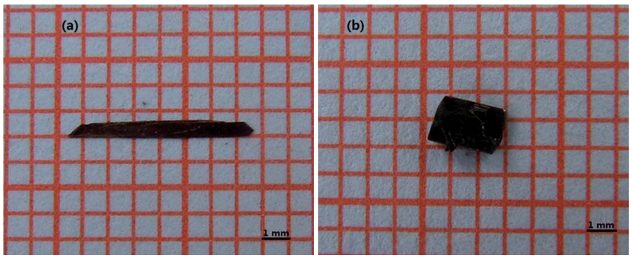

Fig. 5 Bulk single crystals of **3c** and **3i** with sizes of 7 × 1 mm² and 3 × 2 mm² have been grown.

Crystallographic data of **3a**, **3c** and **3i** crystals are listed in Table 2. The crystal structures of **3a**, **3c** and **3i** are monoclinic, **3c** exhibits a noncentrosymmetric crystal structure possessing space group $P2_1$ while **3a** and **3i** crystallize in centrosymmetric structures with space group $P2_1/c$ and $P2_1/n$, respectively. The packing diagrams of **3a**, **3c** and **3i** crystals obtained from X-ray analysis are presented in Fig. 6–8. For ion structures of **3c** and **3i**, disorder was observed in the anion part although the cation structures were determined unequivocally. The chromophore's noncentrosymmetric alignment is a prerequisite for second order optical effects such as second harmonic generation (SHG) and electro-optical modulation. Crystallographic data show that beside the Coulombic interactions between the cation and anion parts, intermolecular and intramolecular hydrogen bonds also play a role in crystal packing and chromophores orientation. There is only one type of hydrogen bond formed between the hydrogen atom of amino and the oxygen atom of sulfonic acid group in **3i** crystals (Fig.9(a)). While in **3c** crystals, the hydrogen-bonded network formed by three kinds of O–H–O hydrogen bonds between the anion layers with H–O distances from 1.802 Å to 2.105 Å (Fig.9(b)). The presence of intermolecular hydrogen bonding may be one of the factors contributing to their high melting points as previously described. **3c**, with a large macroscopic optical nonlinearity of 0.5 times second harmonic generation efficiency of DAST at the non-resonant wavelength of $\lambda =$ 2109 nm, possesses a hydrous phase with a noncentrosymmetric structure while the hydrate of DAST forms a centrosymmetric one. The cation chromophores of **3c** are almost parallel to the x axis and the y axis just as previously described (Fig.7), and glide planes are observed along the diagonal orientation of the structure of **3i** (Fig.8(b)).

Table 2 Crystallographic data of **3a**, **3c** and **3i** crystals

	3a	**3c**·H_2O	**3i**
Formula	$C_{14}H_{17}IN_2S$	$C_{20}H_{24}N_2O_5S_2$	$C_{22}H_{29}N_3O_4S_2$
Formula weight	372.26	436.50	463.60
Crystal system	Monoclinic	Monoclinic	Monoclinic
Space group	$P2_1/c$	$P2_1$	$P2_1/n$
a/Å	10.1143(5)	9.621(7)	7.965(3)
b/Å	20.9362(13)	15.234(11)	16.675(5)
c/Å	14.6323(7)	13.948(10)	17.439(6)
α (°)	90.00	90.00	90.00
β (°)	104.1530(10)	93.85(14)	100.690(5)
γ (°)	90.00	90.00	90.00
V/Å³	3004.4(3)	2040(3)	2276.1(13)
Z	8	4	4

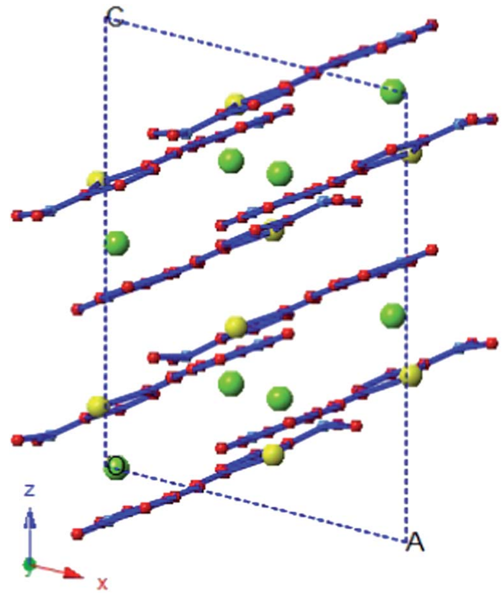

Fig. 6 Crystal packing of **3a** projected along the crystallographic axis y.

Conclusions

A series of thienyl-substituted pyridinium compounds with a variety counter-anions were prepared and their physical properties such as melting points, absorption peaks λ_{max} and SHG activity were studied. By introducing the thienyl group, the new pyridinium derivatives show red-shifted absorption

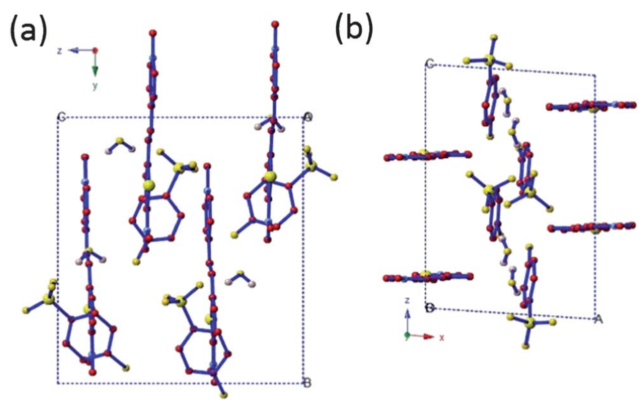

Fig. 7 Crystal packing of **3c** projected along the crystallographic axis x (a) and y (b).

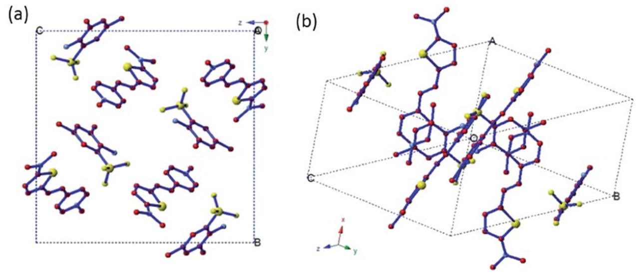

Fig. 8 Crystal packing of **3i** projected along the crystallographic axis *x* (a) and orientation [111] (b).

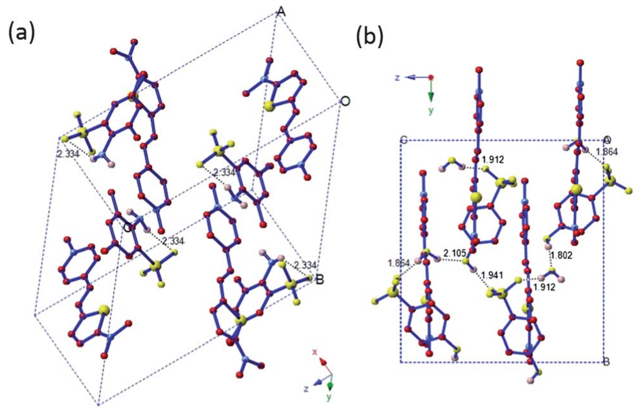

Fig. 9 Crystal packing diagram of **3i** (a) and **3c** (b) projected along the coordinate axis shown in Fig. 9. The molecules are linked by Coulombic interactions between the ionic parts and by hydrogen bonds that are indicated by dotted lines.

maximum compared with the well studied DAST. Kurtz powder tests revealed that, out of the twelve new pyridinium salts, four exhibit noncentrosymmetric structures and the maximum of the powder second-harmonic generation intensities of them is 0.6 times of DAST, implying that the new thienyl-substituted pyridinium salts are a series of promising nonlinear optical materials. Good quality single crystals of **3c** and **3i** were successfully grown from methanol by the slow evaporation method with sizes of 7×1 mm^2 and 3×2 mm^2, respectively. The crystal structure of **3c**, possessing a large macroscopic optical nonlinearity of 0.5 times of that of DAST at the non-resonant wavelength of $\lambda = 2109$ nm, has been determined, and it belongs to the non-centrosymmetric space group $P2_1$. Besides the effect of the cation structures, these results once again reveal that the crystal packing of stilbazolium-like salts is very sensitive to the nature of the counter-anions.[17] Therefore, further modification of the counter-anions is expected to lead to optimized pyridinium salt structures with improved nonlinear optical properties and physical and chemical properties that are important for single-crystal growth and further material processing for applications.

Experimental

Synthesis

All reagents were purchased as high purity from Acros Organics, Aladdin reagents and used without further purification. The products were dried under vacuum for 24 h to remove solvents effectively. ^{1}H NMR spectra were recorded on a Bruker 400 MHz spectrometer on DMSO solutions or $CDCl_3$. UV-vis spectra were recorded by a UV/VIS/NIR spectrophotometer (JASCO V-570). Elemental analyses were performed by Element Analyzer (Flash EA 1112) in Institute of Chemistry Chinese Academy of Sciences. The differential scanning calorimetric (DSC, Perkin Elmer Pyris 6) analysis was used with a heating and a cooling rate of 10 °C min^{-1} under a dry nitrogen purge. The X-ray diffraction was performed by in Rigaku Saturn 724 CCD diffractometer with using Mo-Kα radiation monochromatized with a graphite crystal.

2 ^{1}H-NMR($CDCl_3$, 400MHz) δ = 9.46(s, 2H, CHO), 7.46(d, 1H, J = 4.4 Hz, C_4H_2S), 5.91 (d, 1H, J = 4.4 Hz, C_4H_2S), 3.07(s, 6H, C_2H_6N). Elemental analysis for C_7H_9NOS: (%) calcd C, 54.19; H, 5.81; N, 9.03%. Found: C, 54.12; H, 5.95; N, 8.91%.

3a ^{1}H-NMR(DMSO, 400MHz) δ = 8.49(d, 2H, J = 6.8 Hz, C_6H_4N), 8.04(d, 2H, J = 15.2 Hz, C_2H_2), 7.83(d, 2H, J = 6.8 Hz, C_6H_4N), 7.28 (d, 1H, J = 4.4 Hz, C_4H_2S), 6.46(d, 1H, J = 15.2 Hz, C_2H_2), 6.08(d, 1H, J = 4.4 Hz, C_4H_2S), 4.07(s, 3H, NCH_3), 3.06(s, 6H, C_2H_6N). Elemental analysis for $C_{14}H_{17}IN_2S$: (%) calcd C, 45.17; H, 4.53; N, 7.60%. Found: C, 45.21; H, 4.63; N, 7.48%.

3b ^{1}H-NMR(DMSO, 400MHz) δ = 8.50(d, 2H, J = 6.4 Hz, C_6H_4N), 8.05–8.01(d, 2H, J = 15.2 Hz, C_2H_2), 7.84(d, 2H, J = 6.4 Hz, C_6H_4N), 7.48(d, 2H, J = 8.0 Hz, C_6H_4), 7.28 (d, 1H, J = 4.0 Hz, C_4H_2S), 7.12(d, 2H, J = 8.0 Hz, C_6H_4), 6.48(d, 1H, J = 15.2 Hz, C_2H_2), 6.08(d, 1H, J = 4.4 Hz, C_4H_2S), 4.07(s, 3H, NCH_3), 3.06(s, 6H, C_2H_6N). Elemental analysis for $C_{21}H_{24}N_2O_3S_22$: (%) calcd C, 60.55; H, 5.81; N, 6.72%. Found: C, 60.31; H, 5.88; N, 6.69.

3c ^{1}H-NMR(DMSO, 400MHz) δ = 9.48(s, 1H, OH), 8.49(d, 2H, J = 6.8 Hz, C_5H_4N), 8.04(d, 1H, J = 15.6 Hz, C_2H_2), 7.83(d, 2H, J = 6.8 Hz, C_5H_4N), 7.39(d, 2H, J = 8.4 Hz, C_6H_4), 7.28(d, 1H, J = 4.4 Hz, C_4H_2S), 6.65(d, 2H, J = 8.4 Hz, C_6H_4), 6.46(d, 1H, J = 15.6 Hz, C_2H_2), 6.07(d, 1H, J = 4.4 Hz, C_4H_2S), 4.06(s, 3H, CH_3), 3.06(s, 6H, C_2H_6N). Elemental analysis for $C_{20}H_{22}N_2O_4S_2$: (%) calcd C, 57.39; H, 5.30; N, 6.69%. Found: C, 57.01; H, 5.29; N, 6.67%.

3d ^{1}H-NMR(DMSO, 400MHz) δ = 8.49(d, 2H, J = 6.4 Hz, C_5H_4N), 8.04(d, 1H, J = 15.2 Hz, C_2H_2), 7.84(d, 2H, J = 6.4 Hz, C_5H_4N), 7.60(d, 2H, J = 8.0 Hz, C_6H_4), 7.37(d, 2H, J = 8.0 Hz, C_6H_4), 7.28(d, 1H, J = 4.0 Hz, C_4H_2S), 6.47(d, 1H, J = 15.2 Hz, C_2H_2), 6.08(d, 1H, J = 4.0 Hz, C_4H_2S), 4.07(s, 3H, CH_3), 3.07(s, 6H, C_2H_6N). Elemental analysis for $C_{20}H_{21}ClN_2O_3S_2 \cdot 1/2H_2O$: (%) calcd C, 53.86; H, 4.97; N, 6.28%. Found: C, 53.85; H, 4.85; N, 6.42%.

3e ^{1}H-NMR(DMSO, 400MHz) δ = 10.88(s, 1H, CHO), 8.49 (d, 2H, J = 6.4 Hz, C_6H_4N), 8.05 (d, 2H, J = 15.2 Hz, C_2H_2), 7.84 (m, 3H, J = 11.6 Hz, $C_6H_4N + C_6H_4$), 7.76(t, 1H, J = 7.6 Hz, C_6H_4), 7.61(t, 1H, J = 7.6 Hz, C_6H_4), 7.49(d, 1H, J = 7.6 Hz, C_6H_4), 7.28 (d, 1H, J = 4.0 Hz, C_4H_2S), 6.47(d, 1H, J = 15.2 Hz, C_2H_2), 6.09(d, 1H, J = 4.0 Hz, C_4H_2S), 4.08(s, 3H, NCH_3), 3.07 (s, 6H, C_2H_6N). Elemental analysis for $C_{21}H_{22}N_2O_4S_2$: (%) calcd C, 58.58; H, 5.15; N, 6.51%. Found: C, 58.45; H, 5.19; N, 6.50%.

3f ^{1}H-NMR(DMSO, 400MHz) δ = 8.49(d, 2H, J = 6.8 Hz, C_6H_4N), 8.15(s, 1H, C_6H_3), 8.04(d, 2H, J = 15.2 Hz, C_2H_2), 7.84 (d, 2H, J = 6.8 Hz, C_6H_4N), 7.56(m, 3H, J = 12.0 Hz, NH_2 + C_6H_3), 7.28(d, 1H, J = 4.0 Hz, C_4H_2S), 6.96(d, 1H, J = 8.4 Hz,

C_4H_2), 6.47(d, 1H, $J = 15.2$ Hz, C_2H_2), 6.08(d, 1H, $J = 4.0$ Hz, C_4H_2S), 4.07(s, 3H, NCH_3), 3.06(s, 6H, C_2H_6N). Elemental analysis for $C_{20}H_{22}N_4O_5S_2$: (%) calcd C, 51.93; H, 4.79; N, 12.11%. Found: C, 51.87; H, 4.80; N, 12.09%.

3g ^{1}H-NMR(DMSO, 400MHz) $\delta = 8.49$(d, 2H, $J = 6.8$ Hz, C_5H_4N), 8.32(s, 1H, C_6H_4), 8.19(d, 1H, $J = 8.8$ Hz, C_6H_4), 8.04 (m, 2H, $J = 15.6$ Hz, $C_6H_4 + C_2H_2$), 7.83(d, 2H, $J = 6.4$ Hz, C_5H_4N), 7.66(t, 1H, $J = 15.6$ Hz, C_6H_4), 7.27(d, 1H, $J = 4.4$ Hz, C_4H_2S), 6.46(d, 1H, $J = 15.6$ Hz, C_2H_2), 6.08(d, 1H, $J = 4.4$ Hz, C_4H_2S), 4.07(s, 3H, CH_3), 3.07(s, 6H, C_2H_6N). Elemental analysis for $C_{20}H_{21}N_3O_5S_2$: (%) calcd C, 53.68; H, 4.73; N, 9.39%. Found: C, 53.77; H, 4.69; N, 9.46%.

3h ^{1}H-NMR(DMSO, 400MHz) $\delta = 9.84$(s, 1H, OH), 8.80(s, 1H, OH), 8.49(d, 2H, $J = 6.4$ Hz, C_5H_4N), 8.04(d, 1H, $J = 15.2$ Hz, C_2H_2), 7.83(d, 2H, $J = 6.4$ Hz, C_5H_4N), 7.28(d, 1H, $J = 4.0$ Hz, C_4H_2S), 6.87(s, 1H, C_6H_3), 6.59(m, 2H, $J = 13.6$ Hz, $C_6H_3 + C_6H_3$), 6.47(d, 1H, $J = 15.2$ Hz, C_2H_2), 6.08(d, 1H, $J = 4.0$ Hz, C_4H_2S), 4.07(s, 3H, CH_3), 3.07(s, 6H, C_2H_6N). Elemental analysis for $C_{20}H_{22}N_2O_5S_2$: (%) calcd C, 55.28; H, 5.10; N, 6.45%. Found: C, 54.94; H, 5.12; N, 6.43%.

3i ^{1}H-NMR(DMSO, 400MHz) $\delta = 8.49$(d, 2H, $J = 6.8$ Hz, C_5H_4N), 8.04(d, 1H, $J = 15.2$ Hz, C_2H_2), 7.83(d, 2H, $J = 6.8$ Hz, C_5H_4N), 7.27(d, 1H, $J = 4.4$ Hz, C_4H_2S), 7.13(s, 1H, C_6H_2), 6.72 (s, 1H, C_6H_2), 6.46(d, 1H, $J = 15.2$ Hz, C_2H_2), 6.08(d, 1H, $J = 4.4$ Hz, C_4H_2S), 5.14(s, 2H, NH_2), 4.06(s, 3H, CH_3), 3.06(s, 6H, C_2H_6N), 2.09(s, 3H, CH_3), 2.00(s, 3H, CH_3). Elemental analysis for $C_{22}H_{27}N_3O_3S_2 \cdot H_2O$: (%) calcd C, 56.99; H, 6.30; N, 9.06%. Found: C, 57.04; H, 6.17; N, 9.12%.

3j ^{1}H-NMR(DMSO, 400MHz) $\delta = 8.49$(d, 2H, $J = 6.8$ Hz, C_5H_4N), 8.04(d, 1H, $J = 15.2$ Hz, C_2H_2), 7.83(d, 2H, $J = 6.8$ Hz, C_5H_4N), 7.27(d, 1H, $J = 4.4$ Hz, C_4H_2S), 7.21(s, 1H, C_6H_3), 6.78 (d, 1H, $J = 6.4$ Hz, C_6H_3), 6.47(m, 2H, $J = 18.4$ Hz, $C_6H_3 + C_2H_2$), 6.08(d, 1H, $J = 4.4$ Hz, C_4H_2S), 4.06(s, 3H, CH_3), 3.06(s, 6H, C_2H_6N). Elemental analysis for $C_{21}H_{25}N_3O_3S_2 \cdot 1/2H_2O$: (%) calcd C, 57.25; H, 5.95; N, 9.54%. Found: C, 57.28; H, 5.84; N, 9.42%.

3k ^{1}H-NMR(DMSO, 400MHz) $\delta = 9.52$(s, 1H, OH), 9.14(d, 1H, $J = 8.4$ Hz, $C_{10}H_4N$), 8.82(d, 1H, $J = 8.4$ Hz, $C_{10}H_4N$), 8.49 (d, 2H, $J = 6.4$ Hz, C_6H_4N), 8.04(d, 2H, $J = 15.2$ Hz, C_2H_2), 7.83 (d, 3H, $J = 4.4$ Hz, $C_6H_4N + C_{10}H_4N$), 7.58(d, 1H, $J = 8.4$ Hz, $C_{10}H_4N$), 7.28 (d, 1H, $J = 4.0$ Hz, C_4H_2S), 6.96(d, 1H, $J = 8.4$ Hz, $C_{10}H_4N$), 6.47(d, 1H, $J = 15.2$ Hz, C_2H_2), 6.08(d, 1H, $J = 4.4$ Hz, C_4H_2S), 4.07(s, 3H, NCH_3), 3.06(s, 6H, C_2H_6N). Elemental analysis for $C_{23}H_{23}N_3O_4S_2$: (%) calcd C, 58.85; H, 4.90; N, 8.96%. Found: C, 58.88; H, 4.93; N, 8.96%.

3l ^{1}H-NMR(DMSO, 400MHz) $\delta = 9.80$(s, 1H, OH), 9.58(s, 1H, OH), 8.49(d, 2H, $J = 6.4$ Hz, C_6H_4N), 8.04(d, 2H, $J = 15.2$ Hz, C_2H_2), 7.84(d, 2H, $J = 6.4$ Hz, C_6H_4N), 7.69(d, 1H, $J = 8.8$ Hz, $C_{10}H_5$), 7.46(s, 1H, $C_{10}H_5$), 7.31 (m, 2H, $J = 15.2$ Hz, $C_4H_2S + C_{10}H_5$), 7.04(d, 1H, $J = 17.6$ Hz, $C_{10}H_5 + C_{10}H_5$), 6.47(d, 1H, $J = 15.2$ Hz, C_2H_2), 6.09(d, 1H, $J = 4.0$ Hz, C_4H_2S), 4.08(s, 3H, NCH_3), 3.07(s, 6H, C_2H_6N). Elemental analysis for $C_{24}H_{24}N_2O_5S_2$: (%) calcd C, 59.50; H, 4.96; N, 5.79%. Found: C, 59.36; H, 4.91; N, 5.86%.

SHG measurements

The samples were pressed between glass microscope cover slides and secured with tape in 1-mm thick aluminum holders containing an 8-mm diameter hole. They were then placed in a light-tight box and irradiated with a pulsed infrared beam of wavelength 2109 nm, which is pumped from a Q-switched Nd: YAG laser of wavelength 1064 nm(10 ns, 3 mJ, 10 Hz) by OPO method using a single KTP crystal. A cut-off filter was used to limit background flash-lamp light on the sample, and an interference filter (1050 ± 10 nm) was used to select the second harmonic for detection with a photomultiplier tube attached to a RIGOL DS1052E 50-MHz oscilloscope.

X-Ray crystal structure analysis

Crystal structure data for 3a. $T = 113(2)$K, crystal dimension $0.20 \times 0.18 \times 0.12$ mm^3, μ(Mo-Kα) = 2.256 mm^{-1}. Of 27779 reflections collected in the θ range 1.7°–27.9° using ω and f scans on a Rigaku Saturn724 CCD diffractometer, 7144 were unique reflections. The structure was solved and refined against F^2 using SHELX97, 331 variables, w$R_2 = 0.0467$, $R_1 = 0.0219$, GOF = 1.038, $R_{\text{int}} = 0.0379$.

Crystal structure data for 3c. $T = 113(2)$K, crystal dimension $0.18 \times 0.16 \times 0.14$ mm^3, μ(Mo-Kα) = 0.296 mm^{-1}. Of 17523 reflections collected in the θ range 1.46°–25.03° using ω and f scans on a Rigaku Saturn724 CCD diffractometer, 7038 were unique reflections. The structure was solved and refined against F^2 using SHELX97, 571 variables, w$R_2 = 0.1368$, $R_1 = 0.0637$, GOF = 1.091, $R_{\text{int}} = 0.0662$.

Crystal structure data for 3i. $T = 113(2)$K, crystal dimension $0.22 \times 0.20 \times 0.14$ mm^3, μ(Mo-Kα) = 2.256 mm^{-1}. Of 19233 reflections collected in the θ range 1.7°–25.02° using ω and f scans on a Rigaku Saturn724 CCD diffractometer, 4013 were unique reflections. The structure was solved and refined against F^2 using SHELX97, 398 variables, w$R_2 = 0.561$, $R_1 = 0.0562$, GOF = 1.162, $R_{\text{int}} = 0.0480$.

Acknowledgements

This work was supported by the Natural Science Foundation (Grant No. 50803005), the Fundamental Research Funds for the Central Universities, the Scientific Research Foundation for the Returned Overseas Chinese Scholars, the National Natural Science Fund for Distinguished Young Scholar (Grant No. 51025313).

References

1 K. Yamada, H. Fukuda, T. Tsuchizawa, T. Watanabe, T. Shoji and S. Itabashi, *IEEE Photonics Technol. Lett.*, 2006, **18**, 1046.
2 C. Diederichs, J. Tignon, G. Dasbach, C. Ciuti, A. Lemaitre, J. Bloch, P. Roussignol and C. Delalande, *Nature*, 2006, **440**, 904.
3 C. Gu, Y. Xu, Y. S. Liu, J. J. Pan, F. Q. Zhou and H. He, *Opt. Mater.*, 2003, **23**, 219.
4 M. Samoc, N. Gauthier, M. P. Cifuentes, F. Paul, C. Lapinte and M. G. Humphrey, *Angew. Chem., Int. Ed.*, 2006, **45**, 7376.
5 C. Dorrer, *IEEE J. Sel. Top. Quantum Electron.*, 2006, **12**, 843.
6 S. R. Marder and J. W. Perry, *Science*, 1994, **263**, 1706.
7 Ch. Bosshard, R. Spreiter, L. Degiorgi and P. Günter, *Phys. Rev. B: Condens. Matter*, 2002, **66**, 205107.
8 B. J. Coe, S. P. Foxon, E. C. Harper, J. Raftery, R. Shaw, C. A. Swanson, I. Asselberghs, K. Clays, B. S. Brunschwig and A. G. Fitch, *Inorg. Chem.*, 2009, **48**, 1370.

9 G. Knopfle, R. Schlesser, R. Ducret and P. Günter, *Nonlinear Opt.*, 1995, **9**, 143.
10 F. Pan, G. Knopfle, C. Bosshard, R. Spreiter, M. S. Wong and P. Günter, *Appl. Phys. Lett.*, 1996, **69**, 13.
11 B. Ruiz, Z. Yang, V. Gramlich, M. Jazbinsek and P. Günter, *J. Mater. Chem.*, 2006, **16**, 2839.
12 M. J. Cho, D. H. Choi, P. A. Sullivan, A. J. P. Akelaitis and L. R. Dalton, *Prog. Polym. Sci.*, 2008, **33**, 1013.
13 J. Ogawa, S. Okada, Z. Glavchevab and H. Nakanishi, *J. Cryst. Growth*, 2008, **310**, 836.
14 H. Umezawa, K. Tsuji, S. Okada, H. Oikawa, H. Matsudab and H. Nakanishi, *Opt. Mater.*, 2003, **21**, 75.
15 Z. Yang, S. Aravazhi, A. Schneider, P. Seiler, M. Jazbinsek and P. Günter, *Adv. Funct. Mater.*, 2005, **15**, 1072.
16 Z. Yang, L. Mutter, M. Stillhart, B. Ruiz, S. Aravazhi, M. Jazbinsek, A. Schneider, V. Gramlich and P. Günter, *Adv. Funct. Mater.*, 2007, **17**, 2018.
17 Z. Yang, M. Wörle, L. Mutter, M. Jazbinsek and P. Günter, *Cryst. Growth Des.*, 2007, **7**, 83.
18 Z. Yang, M. Jazbinsek, B. Ruiz, S. Aravazhi, V. Gramlich and P. Günter, *Chem. Mater.*, 2007, **19**, 3512.
19 S. Okada, K. Nogi, Anwar, K. Tsuji, X. M. Duan, H. Oikawa, H. Matsuda and H. Nakanishi, *Jpn. J. Appl. Phys.*, 2003, **42**, 668.
20 J. H. Im, O. P. Kwon, J. H. Kim and S. H. Lee, *Macromolecules*, 2000, **33**, 9606.
21 O. P. Kown, J. H. Im, J. H. Kim and S. H. Lee, *Macromolecules*, 2000, **33**, 9310.
22 B. J. Coe, J. A. Harris, J. J. Hall, B. S. Brunschwig, S. T. Hung, W. Libaers, K. Clays, S. J. Coles, P. N. Horton, M. E. Light, M. B. Hursthous, J. garín and Jesús Orduna, *Chem. Mater.*, 2006, **18**, 5907.
23 P. J. Kim, J. H. Jeong, M. Jazbinsek, S. J. Kwon, H. Yun, J. T. Kim, Y. S. Lee, I. H. Baek, F. Rotermund, P. Güunter and O. P. Kwon, *CrystEngComm*, 2011, **13**, 444.
24 K. Clays and B. J. Coe, *Chem. Mater.*, 2003, **15**, 642.
25 B. J. Coe, J. A. Harris, I. Asselberghs, K. Clays, G. Olbrechts, A. Persoons, J. T. Hupp, R. C. Johnson, S. J. Coles, M. B. Hursthouse and K. Nakatani, *Adv. Funct. Mater.*, 2002, **12**, 110.
26 H. Figi, L. Mutter, C. Hunziker, M. Jazbinsek, P. Günter and B. J. Coe, *J. Opt. Soc. Am. B*, 2008, **25**, 1786.
27 D. Prima, G. Kirscha and J. F. Nicoud, *Synlett*, 1998, 383.
28 F. Würthner, S. Yao, J. Schilling, R. Wortmann, M. R. Abshiro, E. Mecher, F. G. Gomez and K. Meerholz, *J. Am. Chem. Soc.*, 2001, **123**, 2810.
29 S. R. Marder, J. W. Perry and W. P. Schaefer, *Chem. Mater.*, 1994, **6**, 1137.
30 J. Ogawa, S. Okada, Z. Glavcheva and H. Nakanishi, *J. Cryst. Growth*, 2008, **310**, 836.
31 F. Leyder and P. Boulanger, *Bull. Environ. Contam. Toxicol.*, 1983, **30**, 152.